Journal of Applied Polymer Science

Structure-property relationship of substituted pyrrolidine functionalized CNT epoxy nanocomposite

Berhanu Zewde,[1] Praveen Pitliya,[1] Karen J. Gaskell,[2] Dharmaraj Raghavan[1]
[1]Department of Chemistry, Howard University, Washington DC 20059
[2]Department of Chemistry and Biochemistry, University of Maryland, College Park, Maryland
Correspondence to: D. Raghavan (E-mail: draghavan@howard.edu)

ABSTRACT: Carbon nanotubes (CNTs) based polymer nanocomposites hold the promise of delivering exceptional mechanical properties and multifunctional characteristics. However, the realization of exceptional properties of CNT based nanocomposites is dependent on CNT dispersion and CNT-matrix adhesion. To this end, we modified MWCNTs by Prato reaction to yield aromatic (phenyl and 2-hydroxy-4-methoxyphenyl) substituted pyrrolidine functionalized CNTs (fCNT1 and fCNT2) and aliphatic (2-ethylbutyl and n-octyl) substituted pyrrolidine functionalized CNTs (fCNT3 and fCNT4). The functionalization of CNTs was established by Thermogravimetric analysis (TGA), Raman Spectroscopy, and XPS techniques. Optical micrographs of fCNT epoxy mixture showed smaller aggregates compared to pristine CNT epoxy mixture. A comparison of the tensile results and onset decomposition temperature of fCNT/epoxy nanocomposite showed that aliphatic substituted pyrrolidine fCNT epoxy nanocomposites have higher onset decomposition temperature and higher tensile toughness than aromatic substituted pyrrolidine fCNT epoxy nanocomposites, which is consistent with the dispersion results of fCNTs in the epoxy matrix. © 2015 Wiley Periodicals, Inc. J. Appl. Polym. Sci. **2015**, *132*, 42284.

KEYWORDS: composites; mechanical properties; nanotubes; resins; thermal properties

Received 26 January 2015; accepted 31 March 2015
DOI: 10.1002/app.42284

INTRODUCTION

Epoxy resins are widely used in coatings, adhesives, and composites because of their excellent environmental and dimensional stabilities. Additionally, epoxy resins exhibit good bulk properties such as strength, modulus, adhesion to fibers, and hardness. However, epoxy resins suffer from brittleness due to their highly cross-linked structure. An approach to address the brittleness of epoxy resin, is to use 40–60 wt % of glass or carbon fibers as fillers for reinforcement of nanocomposite. Any improvement in toughness of resin is achieved at the expense of increase in the overall density, of composites. To minimize the adverse impact of high % of fiber loading, composites with 0.05 wt % of nanofillers have been formulated, to achieve properties like that of conventional composites.[1] Among the nanofillers, CNTs have drawn specific interest in the field of polymer nanocomposites because of exceptionally high aspect ratio, stiffness, and better stress transfer capability.[2] Potential structural applications of epoxy nanocomposites include aircrafts, and military hardware.

From the structural application point of view, the mechanical and thermal properties of nanocomposites are especially important. Poor interfacial adhesion, inability to transfer the nanotube properties to the resin, agglomeration of CNT, are some of the biggest challenges when dealing with improving the mechanical and thermal properties of nanotube filled polymer composites.[3,4] Typically, 0.05 wt % loading of MWCNTs in epoxy resin is considered adequate to produce high impact resistant composite.[5,6] However, the poorly dispersed state of MWCNTs in epoxy resin limits the translation of excellent mechanical properties of MWCNTs into the filled nanocomposite.[7]

The dispersion of CNTs in epoxy matrix is hindered by the tendency of CNTs to aggregate due to strong Van der waals attraction.[8] Chemical functionalization of nanotubes can promote the dispersability of nanotubes in solvents and/or polymers.[9] The type of substituents on the functionalized CNT surface can also play an important role in the adhesion between nanotubes and polymer. Covalent functionalization, non-covalent functionalization, oxidation by nitric acid-etching, and nitrene chemistry have been used to functionalize CNTs.[10,11] Among the various functionalization methods, 1, 3 dipolar cycloaddition offers unique advantages such as higher graft density of organic functionalities on the CNT surface, and ability to introduce multiple substituents on the pyrrolidine ring in one step synthesis by varying type of amino acids and aldehydes.[11,12] In the past, attempts have been made to chemically couple the amine moieties of functionalized CNT with the epoxy matrix.[13] However, systematic studies are lacking to establish the

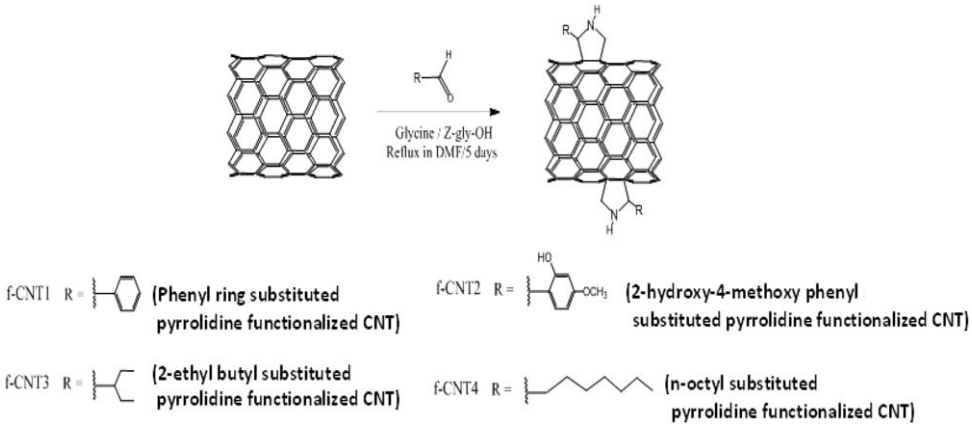

Scheme 1. Schematic of functionalization of MWCNTs.

correlations between the type of CNT functionalization groups, degree of functionalization, processing aspects of CNT/epoxy nanocomposites and their overall properties.[9]

Despite advances in incorporating desired functional groups on CNT, engineering good dispersion of fCNTs in resin remains a challenge. Solvent based methods have been studied to homogeneously disperse CNTs in resin.[14] Use of solvent in processing of nanocomposite is noted to facilitate dispersion of CNTs in the matrix, however, residual solvent in the final composite can adversely affect the overall properties of the nanocomposite.[15] Alternatively, solvent-free processing methods (extrusion, shear mixing, high pressure homogenizer, calendaring, and three roll mill) have been studied to formulate nanocomposites. However, the use of high shear mixing method such as planetary shear mixing to deagglomerate CNTs in polymer nanocomposites has not been exhaustively investigated. In our recent publication, we have demonstrated the effectiveness of planetary mixing method and its combination with sonication in achieving stable dispersion of pristine CNT in epoxy resin.[7] This study aims at achieving good dispersion of fCNT/epoxy mixture using a combination of (planetary mixing + ultra sonication) techniques.

Here, we adopted 1, 3 dipolar cycloaddition reaction for functionalization of CNTs so as to introduce pyrrolidine ring with appropriate substituents on CNTs. Aromatic (phenyl and 2-hydroxy-4-methoxyphenyl) and aliphatic (n-octyl and 2-ethylbutyl) substituents were introduced on pyrrolidine ring of fCNTs. The fCNTs were characterized by use of Raman, TGA, and XPS. Using a combination of planetary shear mixing method and ultra-sonication, the fCNTs were dispersed in epoxy resin. Optical microscopy was used to evaluate the micro-scale dispersion of CNT aggregates. By evaluating the thermal and mechanical properties of epoxy/fCNT nanocomposite and comparing it with pristine epoxy, we establish the role of substituents present on fCNTs on the overall tensile toughness and onset decomposition temperature of nanocomposites.

EXPERIMENTAL

Materials

Epon 862 epoxy resin was supplied by Momentive. Curing agent m-phenylenediamine (MPDA, 99%) and 2-ethylbutyraldhyde (98%) were purchased from Acros Organics and used as received. Pristine multiwall CNTs (carbon > 95%, O.D. × L 6–9 nm × 5 μm, number of walls were 3–6, median tube diameter was 6.6 nm), glycine, N-benzyloxycarbonylglycine (Z-gly-OH), and 2-hydroxy-4-methoxybenzaldhyde were purchased from Sigma Aldrich and used as received. All solvents including, DMF, methanol, and acetone were supplied by Fisher Chemicals. Planetary shear mixer also known as Thinky Mixer ARE 310 was purchased from Thinky Corporation USA, while ultrasonicator was purchased from Branson sonic dismembrator.

Functionalization of MWCNTs. Functionalization of MWCNTs was carried out by using (1, 3 dipolar cycloadddtion) Prato reaction as illustrated in Scheme 1. Briefly, a mixture of glycine (1.426 g), MWCNT (0.054 g), and benzaldehyde (0.95 ml) was dissolved in DMF. The mixture was refluxed for 5 days. After completion of the reaction, the mixture was centrifuged (5000 rpm, 10 min) and the supernatant was discarded. The recovered CNT was subjected to three cycles of washing and centrifugation with methanol and acetone to obtain fCNT1. The resulting black powder was dried under vacuum for 1 day and characterized for composition by XPS, Raman, and TGA. Similarly, for synthesizing fCNT2, only the aldehyde used in the aforementioned procedure was replaced by 2-hydroxy-4-methoxybenzaldhyde. fCNT3 and fCNT4 was synthesized by using modified Paiva *et al.*,[16] procedure by reacting Z-gly-OH (0.502 g) with 2-ethylbutyraldehyde (1.5 ml) and octanal (1.9 ml), respectively.

Preparation of Epoxy/fCNTs Nanocomposite. Initially, 99.95 wt % epoxy and 0.05 wt % MWCNTs (pristine, fCNT1, fCNT2, fCNT3, and fCNT4) were mixed with sonic dismembrator for 30 min and degassed under vacuum to remove any air bubbles from the mixture. Next, 30 wt % of m-Phenylenediamine (MPDA) was added to the mixture and subjected to high speed mixing using ARE 310 Thinky Mixer at 2000 rpm for 30 min to obtain a homogenous mixture. Then the mixture was cured using the protocol described below. Pure epoxy and pristine CNT-epoxy samples were processed using a similar mixing protocol and they served as controls for the study. Additionally, samples with 0.1 wt % fCNTs were prepared to study the effect of fCNT loading on the performance of the nanocomposites.

The processed mixture was degassed under vacuum at 30°C for 10 min. A portion of the mixture was initially coated on dog

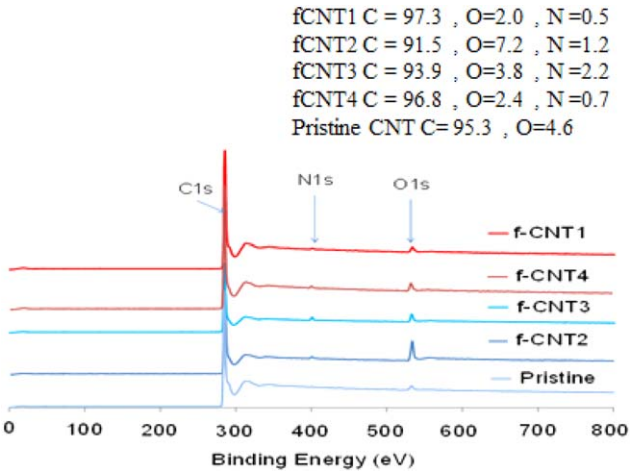

Figure 1. XPS survey spectra and elemental % composition of pristine CNT, fCNT1, fCNT2 fCNT3, and fCNT4. [Color figure can be viewed in the online issue, which is available at wileyonlinelibrary.com.]

bone shaped silicone rubber mold and degassed for 20 min under vacuum. Then the bulk mixture was poured on the mold and further degassed for 20 min prior to placing in a programmable oven (Thermofisher). Curing was initiated by ramping the oven temperature from room temperature to 121°C at 2°C min^{-1} and holding the sample at 121°C for 2 h followed by cooling the sample to room temperature overnight. Similar protocol was followed to cure pristine epoxy. The cured samples were retrieved and saved for thermal and mechanical measurements.

Raman Characterization of fCNTs. Raman measurements of the fCNTs and pristine CNTs were performed with an excitation laser wavelength of 532 nm and a 1200 L/mm grating using an ExamineR Nuspec, Deltanu, and Raman Microspectrometer. Data analysis and curve fitting were performed using Nustec software. To collect Raman spectra, CNT and fCNTs were dispersed in hexane using sonicator and a drop of the dispersion was placed on silicon glass and air dried.

XPS Characterization of fCNTs. The surface composition of fCNTs and pristine CNT was obtained by performing XPS measurement with Kratos Axis 165 X-ray Photoelectron Spectrometer, using mono-chromatic Al(K_α) source at 260 W. Charge neutralization was required to prevent surface charge build up. Binding energies were charge corrected to 284.3 eV for the sp^2 hybridized carbon of the CNT. XPS facility at the surface analysis center of University of Maryland College Park was used.

TGA Characterization of fCNTs and fCNT/Epoxy Nanocomposite. Thermogravimetric analysis (TGA) of the fCNTs and pristine CNT was conducted using a TGA/DTA 320 Seiko instrument in a nitrogen atmosphere (flow rate of 100 ml/min). The thermogram was generated by placing nearly 10 mg of CNT (pristine, fCNTs) in a pan and heating it from 30°C to 100°C at a rate of 10°C min^{-1} and maintaining the sample at 100°C for 30 min; then ramping it from 100°C to 600°C at a rate of 10°C min^{-1}. Similar protocol was used for thermal analysis of fCNT/epoxy nanocomposite and pure epoxy.

Optical Microscopy of CNT/Epoxy Mixture. A droplet of the uncured CNT/epoxy mixture was placed on glass slide and observed by Keyence Digital Microscope multiscan VHS 1000E in transmission light mode. A 5000 X objective lens was used to collect images of the uncured mixture. NIH Image J software was used to obtain semiqualitative information about CNT dispersion in the matrix.

Tensile Testing of CNT/Epoxy Nanocomposite. Tensile tests were performed according to modified ASTM standards protocol. The dimensions of dog-bone specimens were 25 mm (length) × 4 mm (gauge width) × 1.8 mm (thickness). Tensile experiments were conducted on an Instron 5569 A tensile tester equipped with 50 KN load cell capability at room temperature using a cross-head speed of 2.54 mm/min. A small preload was applied to prevent slippage of the specimen prior to performing actual tensile measurements.

RESULTS AND DISCUSSION

XPS Measurements of fCNTs

XPS measurements were performed on pristine CNT and fCNTs so as to establish that the CNT has been functionalized with a substituted pyrrolidine moiety. Figure 1 shows the survey scan of pristine CNT and fCNTs. The survey scan of the pristine CNT showed characteristic peaks of C 1s at 284.3 eV and a weak peak for O 1s at 530 eV. The oxygen functionality may have been incidentally incorporated during purification (processes used to remove amorphous carbon and residual metal) of pristine CNT or exposure of pristine CNT to environmental oxidants.[17]

XPS survey scan of fCNT2 exhibits a strong oxygen peak (the O content was 7.0 at.%) which can be attributed to the introduction of –OH and $–OCH_3$ groups on the CNT surface. However, in the case of other fCNTs, the oxygen content did not change considerably with respect to pristine CNT increasing from 2.5 to 3.0 at %. The appearance of the nitrogen signal at 400.2 eV in each of the fCNTs is evidence of formation of pyrrolidine ring on CNT surface. Since the fCNTs were extensively washed and centrifuged, the likelihood of unreacted glycine contributing to C–N peak in the fCNTs was considered improbable.

Figure 2 shows the high resolution C1s region of all fCNTs compared to a pristine CNT. The pristine CNT shows a peak at 284.3 eV with a tail towards the higher binding energy and low intensity $\pi \rightarrow \pi^*$ shake-up satellite peaks at 291 and 294 eV, this peak shape is characteristic of graphitic carbon, (π-conjugated carbon system) as expected for a CNT. The sampling depth of XPS in the C 1s region was ~ 6nm, (graphite at 1203 eV, NIST Standard Reference Database 71). Therefore we probed not only the outer functionalized wall but also the unfunctionalized inner walls. On first inspection the C 1s peak shape of the fCNTs looks very similar to that of the pristine, as may be expected due to the relatively small number of total carbons that are functionalized. The C 1s region was peak fit in a manner to highlight the change in peak shape upon functionalization as compared to the pristine nanotube and this was achieved by performing a peak fit for the fCNTs that included the line-shape of the pristine CNT as one of the components (labeled as CNT in Figure 2). Three additional components included in the fit were constrained to have equal

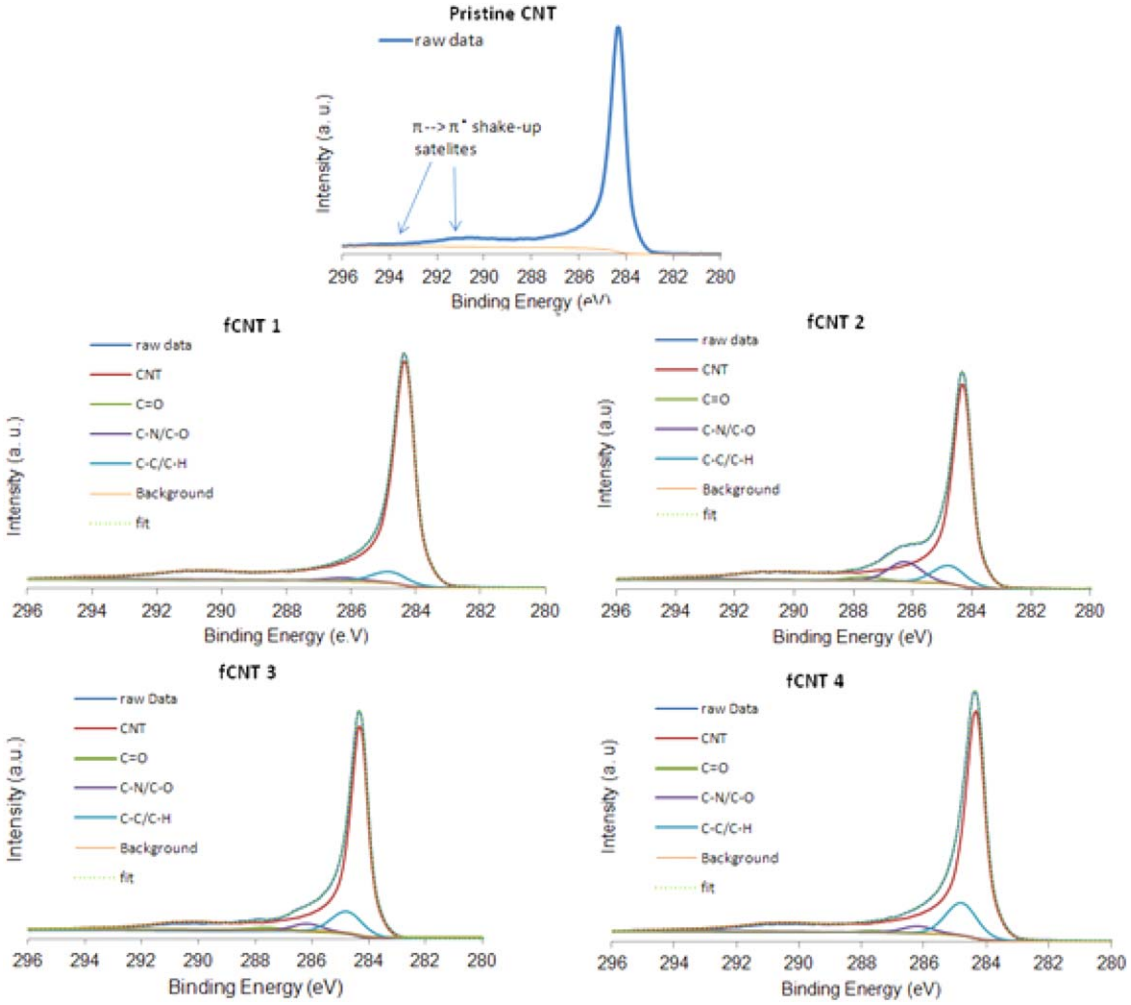

Figure 2. C 1s core level spectra of fCNT1, fCNT2, fCNT3, and fCNT4. [Color figure can be viewed in the online issue, which is available at wileyonlinelibrary.com.]

FWHM and fixed binding energy with sp^3 carbon (C–C/C–H, Figure 2) at 284.8 eV, C–O and C–N bonding at 286.2 eV, and C=O at 287.7 eV. Relative percentage composition of C 1s bonding environments derived from the peak fits can be found in Table I. It is not possible to distinguish between C–N and C–O bonding in the C 1s, therefore, the relative % of C–N/C–O bonding calculated from the peak fit for fCNT 1, fCNT 3, and fCNT 4 scales relatively well with the total amount of nitrogen (Figure 1), inferring the majority of the area in this component is from the C–N bonding which is consistent with the incorporation of the pyrrolidine ring moieties on the surface of the CNT. The area of the C–N/C–O peak (8.6%) is much larger for fCNT2 this is consistent with the incorporation of not only the nitrogen from the pyrrolidine ring but also the C–O bonding methoxy and hydroxyl groups of the attached molecule.

Table I. Relative Percentage Composition Derived from XPS C 1s Peak Fit

Sample	CNT (%)	C-C/C-H (%)	C-N/C-O (%)	C=O (%)
fCNT1	93.3	5.1	1.3	0.3
fCNT2	81.4	8.2	8.6	1.8
fCNT3	85.2	9.9	3.7	1.2
fCNT4	85.0	11.8	2.4	0.7
Pristine	100.0	-	-	-

Further evidence of the successful incorporation of the different functional groups comes from the relative areas of the sp^3 C–C/C–H peak areas (Table I), i.e. the peak area increases as expected as the number of sp3 carbons in the functional group attached to the pyrrolidine ring increases.

To establish that pyrrolidine ring is indeed contributing to the C–N component in C 1s scan of fCNTs, we also looked at the high resolution N 1s XPS spectra (not shown here). For all fCNTs, we observed the emergence of a single N 1s peak at 400.2 eV, which is in good agreement to 400.0 eV reported for polypyrole which has an equivalent chemical environment around the nitrogen.[18] Since all fCNTs showed only one peak at 400.2 eV, it appears that we have synthesized cyclic pyrrolidine fCNTs without substituent at N position.[16] The XPS results (N peak at 400.2 eV and C–N peak at 286.2 eV), suggest that we have successfully functionalized CNTs.

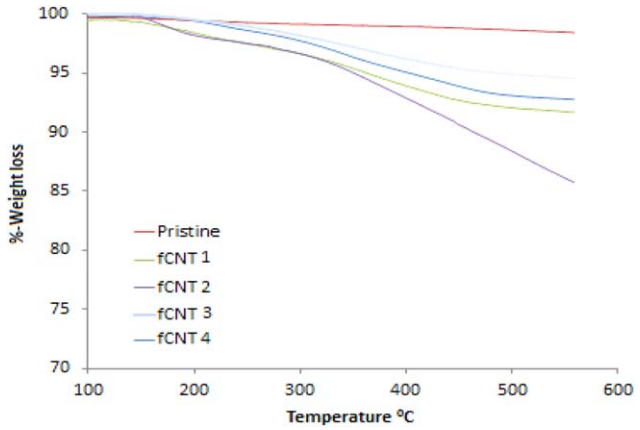

Figure 3. Thermograms of pristine CNT, fCNT1, fCNT2, fCNT3, and fCNT4. [Color figure can be viewed in the online issue, which is available at wileyonlinelibrary.com.]

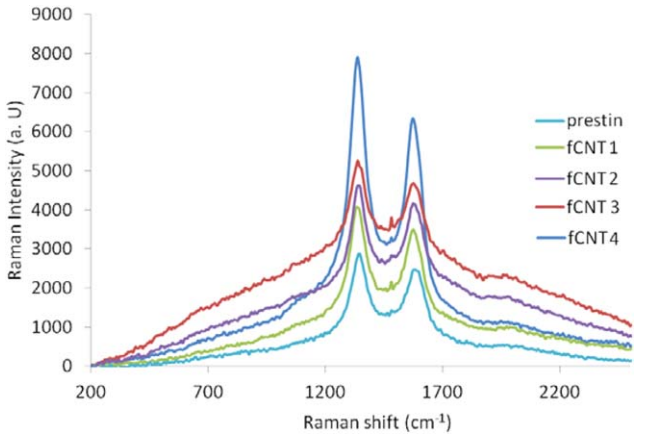

Figure 4. Raman spectra of pristine and functionalized carbon nanotubes. [Color figure can be viewed in the online issue, which is available at wileyonlinelibrary.com.]

Thermal Analysis of fCNTs

Figure 3 shows the thermograms of fCNTs and pristine CNT. A minimum of triplicate measurements were recorded for each specimen. fCNTs exhibit a significant reduction in onset decomposition temperature as compared to pristine CNT (600°C) which can be attributed to the decomposition of organic functionalities prior to the breakdown of CNT backbone.[19] Among fCNTs, fCNT1 and fCNT2 were found to have lower onset decomposition temperature (temperature at which 5 wt % of the initial mass is lost) and higher mass loss (as determined at 500°C), probably because of the decomposition of the phenyl ring attached to the pyrrolidine ring. Similar results have been reported by Grassi *et al.*,[20] where they observed the release of cationic phenyl fragments ($C_6H_5^+$ (m/z = 78) and $C_6H_5^+$ (m/z = 77) based on MS analysis) during thermal breakdown of fCNT1.

Table II lists the mass loss of fCNTs at 500°C and moles of grafted chains decomposed per unit weight of CNT. In our calculation, we assumed the pyrrolidine ring attached to CNT to remain intact up to 500°C based on Grassi *et al.*,[20] observation where it was noted that substituents attached to pyrrolidine decomposes before 500°C, with pyrrolidine ring attached to CNT being intact. For calculating moles of grafted chains, the char residue for fCNT was subtracted from char residue of pristine CNT at 500°C and the differential mass loss was divided by molar mass of the appropriate substituents attached to pyrrolidine ring of fCNT. We observed the graft density of fCNTs to range from 0.05 to 0.09 moles/g of CNT. Small variation in the moles of grafted chain in fCNTs was expected and can be attributed to the reactivity of glycine and aldehyde towards CNT.

Raman Measurements of fCNTs

Figure 4 shows the Raman spectra of pristine CNT and fCNTs. Clearly, the pristine CNT exhibits D band at ~1350 cm^{-1} and G band at 1600 cm^{-1}, which can be assigned to the defects and in-plane vibrations of the graphitic wall of CNT, respectively. The position of G band is sensitive to charge transfer interactions and any alteration to the CNT sp^2 graphitic structure. A frequency shift in G band of fCNTs was noticed compared to pristine CNT which indicates that there is the introduction of sp^3 carbon atom in CNT backbone. Highest frequency shift (1600 to 1555 cm^{-1}) was observed for fCNT2 followed by fCNT1 (1600 to 1559 cm^{-1}) and the least frequency shift was for fCNT3 (1600 to 1571 cm^{-1}) and fCNT4 (1600 to 1569 cm^{-1}). Significant shift in G band of fCNT1 and fCNT2 can be a result of $\pi - \pi$ interaction between aromatic substituent and CNT back bone.[21,22] Since Raman scattering is sensitive to the electronic structure, these results serve as another evidence for chemical functionalization of CNT. Even though the Raman frequency shifted to lower wavenumber and the peaks broadened, the Intensity of D band/Intensity of G band did not change significantly. This may be largely interpreted as side wall functionalization of CNT by Prato reaction.[23,24]

Table II. Density of Grafted Substituent on CNT Based on TGA Analysis

Functionalization	Char residue (%) 500°C	Differential mass loss (g)	Molar mass of substituents on CNT (g mol^{-1})[a]	Mole of substituent g^{-1} of CNT	Onset decomposition temperature (°C)
Pristine CNT	98.5				
fCNT1	92.0 ± 1.00	4.00 ± 1.00	77	0.05	362 ± 1.26
fCNT2	87.5 ± 1.00	11.0 ± 1.00	123	0.09	350 ± 4.00
fCNT3	96.0 ± 1.00	5.50 ± 1.00	71	0.08	485 ± 2.90
fCNT4	93.5 ± 1.00	6.50 ± 1.00	99	0.06	402 ± 2.00

[a] Molar mass of the substituent on the pyrrolidine ring.

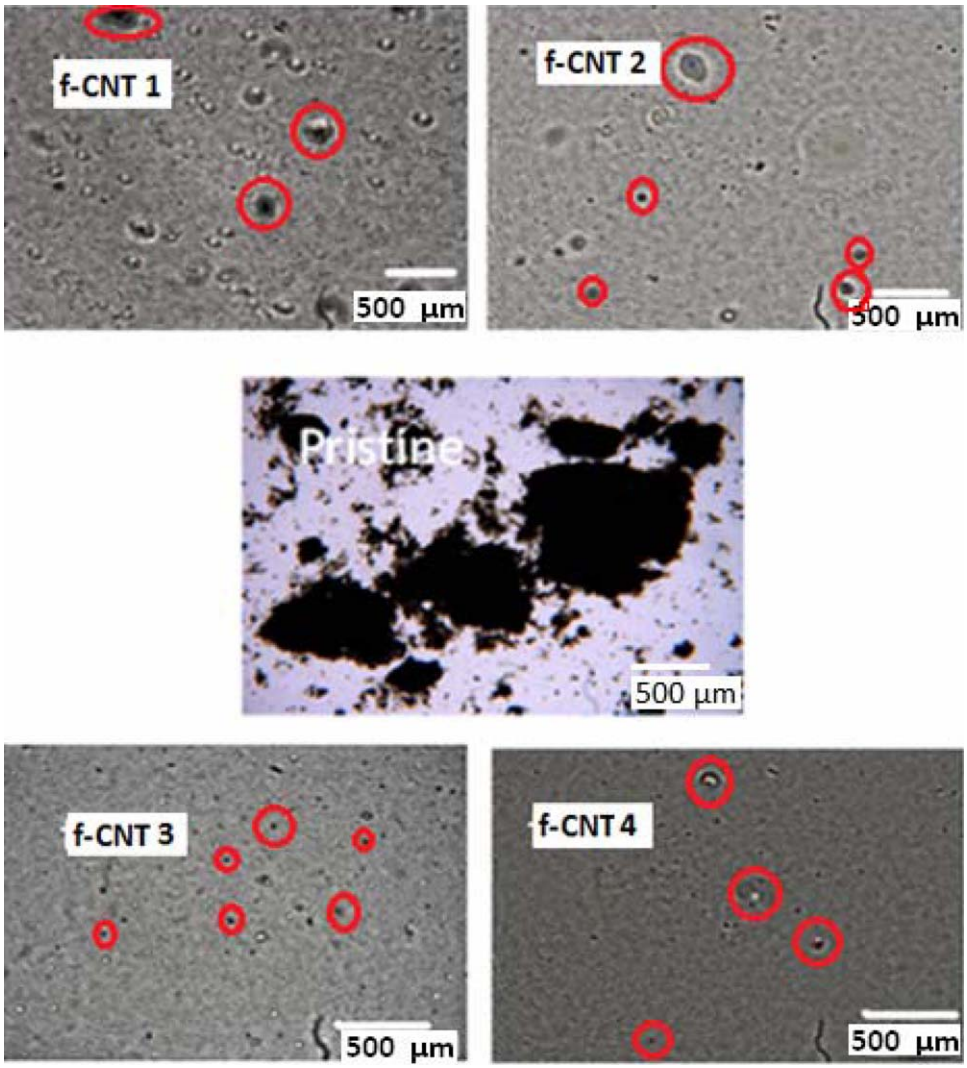

Figure 5. Optical micrographs of uncured CNT/epoxy and fCNT/epoxy mixtures. [Color figure can be viewed in the online issue, which is available at wileyonlinelibrary.com.]

Optical Microscopy Characterization of fCNT/Epoxy Mixture

Figure 5 shows a montage of uncured pristine CNT and fCNT epoxy mixtures, prepared under similar conditions. The images shown are from representative regions of droplets of the liquid mixture placed on a glass covered with coverslip. For proper comparison of mixtures, a fixed loading of CNTs (0.05 wt %) was used preparing the various mixtures. The dark spots in the image indicate CNT aggregates. Our definition of dispersion is based on the size and/or the number of aggregates observed in the mixtures. For pristine CNT/epoxy mixture, we observed large dark spots randomly distributed throughout the specimen along with significant section of the mixture with less visibly dark spot. An image with less visibility. An image not easily visible dark spots does not necessarily imply absence of aggregates instead aggregates are small in size to be observed using optical microscopy.[25]

To assist in the semi-qualitative comparison of the dispersion data, we resorted to NIH Image J analysis of the optical images presented in Figure 5. Note a minimum of 3 images were analyzed to draw CNT dispersion data. Figure 6 shows the distribution of CNT aggregates for the various CNT/epoxy mixtures. We see a bell shaped curve and a tail towards the higher size aggregates. Interestingly, we noticed the bell shaped curve shift from small aggregates to larger aggregates depending on the type of fCNT/epoxy mixture. For example, the fCNT4/epoxy mixture had predominantly the smallest size aggregates while fCNT1/epoxy mixture had predominantly the biggest CNT aggregates. The average aggregates radius for fCNT1/, fCNT2/, fCNT3/ and fCNT4/epoxy mixture was ~27.0 μm, ~74.0 μm, ~102.0 μm, and ~128.0 μm, respectively. These results suggest that the alkyl substituents on the pyrrolidine ring of fCNT, especially the straight chain alkyl substituent is playing an effective role in debundling and dispersing the nanotubes throughout the epoxy matrix.

MECHANICAL PROPERTIES OF NANOCOMPOSITES

Figure 7 shows the representative stress strain curve for the pure epoxy and epoxy nanocomposites when loaded with 0.05 % CNT/epoxy nanocomposite. In order to obtain statistically representative information of tensile stress, toughness, and

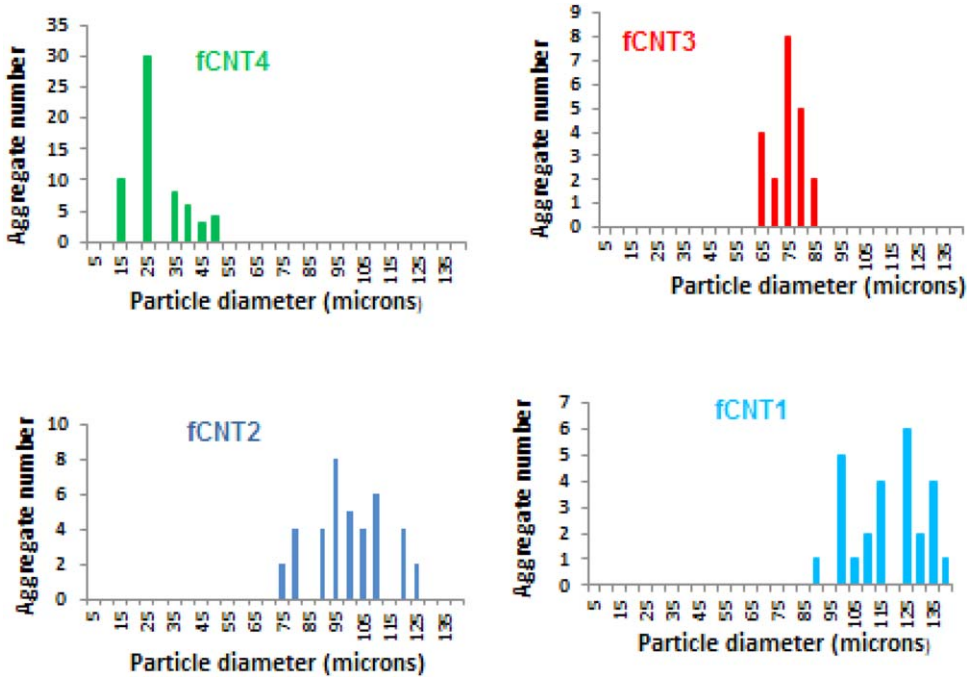

Figure 6. Particle size distribution in various fCNT/epoxy mixtures. [Color figure can be viewed in the online issue, which is available at wileyonlinelibrary.com.]

modulus of the samples, a minimum of 10 specimens from each batch were considered and the specimens that broke beyond the gauge region were not considered for data analysis. Table III summarizes the mechanical data obtained from stress strain curve as a function of type of CNT and CNT loading in the nanocomposite. We applied students t-test to the data of the nanocomposites to establish the 95% confidence level at which the results statistically differ from epoxy. For neat epoxy, stress values exceeding 60 MPa were measured. The incorporation of pristine CNT into epoxy decreased the tensile strength and tensile toughness. The reduction of tensile strength and toughness of nanocomposite is probably a result of CNT aggregates acting as defects in the specimen.

With the incorporation of fCNTs in the epoxy matrix, the tensile stress and tensile toughness increased for all the nanocomposites, regardless of the % loading of CNT. In general, the tensile stress at failure was found to be maximum for fCNT4 nanocomposite (90.7 MPa) followed by fCNT3 nanocomposites, then fCNT2 nanocomposite and the least was for fCNT1 nanocomposite. The results are shown in Table III. Our tensile stress values are in accordance with previously reported value for 0.1 wt % functionalized CNT/epoxy nanocomposite.[33–35] Similar trend was noticed for tensile toughness where the tensile toughness of the fCNT4 nanocomposite was found to be highest (478 MPa) and fCNT1 nanocomposite was found to be the lowest (143 MPa). Commonly, the explanation put forth for enhancement of tensile toughness for nanocomposites is that the nanomaterial acts as reinforcement and the extent of reinforcement depends on the dispersion state of nanomaterials in the matrix and CNT-epoxy adhesion. Our tensile toughness results of nanocomposites strongly corroborates with the dispersion results obtained for various nanocomposites from optical microscopy. Samples with smaller CNT aggregates showed higher tensile toughness (fCNT4 and fCNT3 nanocomposites) while samples with larger CNT aggregates showed lower tensile toughness (fCNT2 and fCNT1 nanocomposites).

The observed trend in mechanical properties of nanocomposites and dispersion state of CNTs in epoxy matrix can possibly be related to the type of functionality present on fCNTs. In pristine CNT/epoxy nanocomposite, the dispersion of CNTs in epoxy matrix is hindered by the tendency of CNTs to aggregate due to strong Van der waals attraction ($\pi - \pi$ interaction among neighboring CNTs), hence the inferior performance of pristine CNT-epoxy nanocomposite.[26] Chemical functionalization of nanotubes is believed to promote the dispersability of nanotubes in polymers, depending on the selection of the functional groups on functionalized nanotubes.[9] Aliphatic substituents on the pyrrolidine functionalized CNTs can minimize the strong $\pi - \pi$

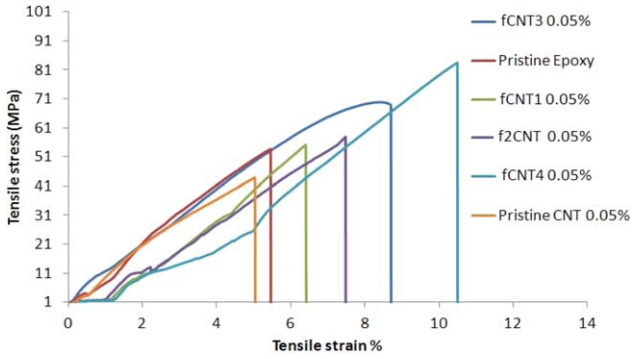

Figure 7. Stress-Strain curve of epoxy, 0.05wt % of CNT epoxy nanocomposite. [Color figure can be viewed in the online issue, which is available at wileyonlinelibrary.com.]

Table III. Summary of Mechanical Properties of Nanocomposite

Sample	Weight (%)	Tensile stress at breaking (MPa)	Tensile toughness (area under curve) (MPa)
fCNT1 Epoxy	0.05	55.2 (±0.38)	143 (±4.40)
	0.10	62.0 (±0.34)	183 (±2.71)
fCNT2 Epoxy	0.05	57.7 (±0.37)	190 (±3.78)
	0.10	64.7 (±0.78)	212 (±4.65)
fCNT3 Epoxy	0.05	69.7 (±0.40)	348 (±5.45)
	0.10	85.3 (±0.46)	380 (±5.25)
fCNT4 Epoxy	0.05	83.6 (±0.43)	366 (±5.10)
	0.10	90.7 (±0.22)	478 (±3.60)
Pristine CNT	0.05	43.0 (±0.28)	106 (±4.12
	0.1	46.9 (±0.31)	125 (± 4.8)
Epoxy	N.A	53.7 (±0.63)	136 (±4.28)

All the nanocomposites when compared with pristine epoxy showed statistically significant difference as established by t-test.

interaction among neighboring CNTs and promote accessibility of the epoxy resin to the amine group present on the pyrrolidine ring of fCNTs so as to promote epoxy-CNT adhesion.[27,28] Especially, the long straight chain alkyl substituent on fCNT4 is expected to significantly enhance the spacing between neighboring CNTs and promote resin diffusion so as to achieve improved dispersion and enhanced tensile toughness. On the other hand, the short branched chain alkyl substituent in fCNT3 can bent on the CNT surface and hinder the spacing between neighboring CNTs and limit resin diffusion. Therefore, we notice a difference in tensile toughness data of fCNT3 nanocomposite and fCNT4 nanocomposite. Aromatic substituted CNT (fCNT1 and fCNT2) nanocomposite showed inferior performance than aliphatic substituted CNT (fCNT3 and fCNT4) nanocomposites. This is because in fCNT1 nanocomposite there is favorable $\pi - \pi$ interaction between aromatic substituents and neighboring CNTs. Aromatic substituents can induce enhanced interaction between neighboring CNTs can reduce the access of epoxy resin to fCNTs and minimize the epoxy-CNT adhesion. While, for fCNT2 nanocomposite, the presence of –OH group on phenyl substituent can play an important role in promoting the hydrogen bond formation with the cured epoxy matrix.[29] These favorable interactions can likely explain the improved tensile toughness of fCNT2-epoxy nanocomposites compared to fCNT1-epoxy nanocomposites. In summary, our results indicate that long chain aliphatic substituent on pyrrolidine ring of fCNTs is more desirable in improving the performance of fCNT nanocomposite. Our explanations put forth should be viewed with caution because of a small selection of functional groups used in the study. Future studies should include a larger selection of functional groups so as to confirm the observed trend on the role of substituents in pyrrolidine functionalized CNTs in influencing the overall mechanical properties of nanocomposites. Also, at present, we do not have any information about orientation of CNT in our nanocomposites which could be important in the overall performance of nanocomposite. In this regard, studies are underway to obtain information about the alignment of CNTs in the processed nanocomposites and this will be reported in future publication.

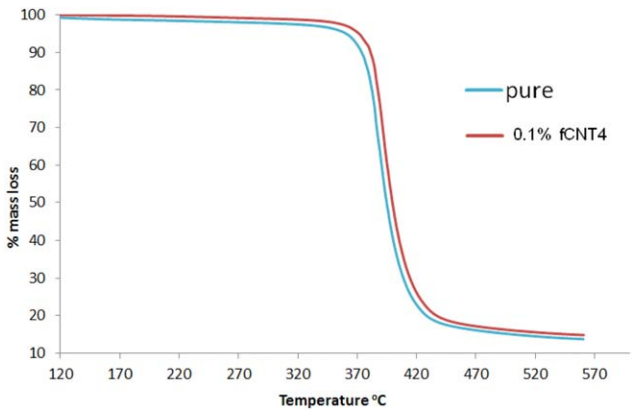

Figure 8. TGA thermograms of neat epoxy and nanocomposites of 0.10 wt % fCNT4. [Color figure can be viewed in the online issue, which is available at wileyonlinelibrary.com.]

Thermal Properties of CNT/Epoxy Nanocomposite

Figure 8 is the thermograms of cured epoxy and fCNT4 nanocomposites when subjected to a heating rate of 10°C/min under a nitrogen atmosphere. The thermograms of all nanocomposites and pristine epoxy is presented in Figure S1. A minimum of triplicate measurements were performed to check the data reproducibility. We compared the char residue of the pure epoxy and fCNT4 nanocomposites at 600°C and it was found to be $13.7 \pm 0.07\%$ and $14.6 \pm 0.08\%$, respectively. The small increase in the char yield of fCNT4/epoxy nanocomposite compared to pure epoxy is a result of the contribution of functionalized CNT towards the char formation in the sample.

Among the various nanocomposites studied, we observed a maximum increase in the onset temperature for fCNT4 nanocomposites ($371°C \pm 0.11°C$) compared to neat epoxy ($361°C \pm 0.24°C$). Similar increase in the onset decomposition temperature of nanocomposite has been reported previously for fCNT nanocomposite.[30] These results suggest the role of

aliphatic substituents on pyrrolidine functionalized CNT in influencing CNT dispersion and possibly interaction of CNT with epoxy resin. The higher the interaction of fCNT4 with the matrix, higher would be the reduction in the mobility of the matrix material around the CNTs.[31] An enhanced thermal stability of fCNT4/epoxy nanocomposite is consistent with our previous observation i.e. the long alkyl chain substituted pyrrolidine functionalized CNT is influencing CNT dispersion, and promoting enhanced overall performance of the nanocomposite.[32]

CONCLUSION

In this study, the role of substituent (aromatic and aliphatic) on fCNTs in influencing the thermal and mechanical properties of CNT/epoxy nanocomposite was investigated. Various substituents were covalently tagged on CNT via Prato reaction and fCNT was characterized using TGA, XPS, and Raman spectroscopy. An appearance of N peak at 400.2 eV and C–N peak at 286.2 eV in XPS and a frequency shift of the G band in Raman spectra for all fCNTs with respect to pristine CNT suggest the successful modification of CNT. In addition the intensity of the Sp3 carbon in the C 1s spectrum was seen to be consistent with the differing amounts of Sp3 carbon in the functional groups. Optical micrographs of the uncured fCNT/epoxy mixtures indicate that fCNT4/epoxy mixture had predominantly the smallest size aggregates among the mixtures studied. The mechanical properties (tensile toughness) of nanocomposites show strong correlation with aggregate size and CNT dispersion in epoxy matrix. Likewise, we noticed fCNT4-epoxy nanocomposite exhibits the highest onset decomposition temperature with respect to pristine epoxy. The superior performance of aliphatic substituted pyrrolidine functionalized CNT nanocomposite compared to aromatic substituted pyrrolidine functionalized CNT nanocomposite can largely be attributed to the effective dispersion of CNT in the epoxy resin. Future studies should include a larger selection of fCNTs so as to confirm our observations of the role of substituents in pyrrolidine functionalized CNTs in influencing the overall mechanical and thermal properties of nanocomposites.

ACKNOWLEDGMENTS

Authors gratefully acknowledge financial support from US Army Research Office grant (5710003423) through ISN at MIT, Boston, MA. Prof. Hosten and Mr. Otchere – Adjei from HU are acknowledged for Raman measurements. We thank Prof. Whitworth and Prof. Owolabi from HU for providing access to Instron instrument (NSF grant 1229082). We also would like to thank Momentive for providing Epon 862.

REFERENCES

1. Eitan, A.; Dukes, D.; Andrews, R.; Schadler, L. S. *Chem. Mater.* **2003**, *15*, 3198.
2. Rahmanian, S.; Suraya, A. R.; Shazed, M. A.; Zahari, R.; Zainudin, E. S. *Mater. Des.* **2014**, *60*, 2014.
3. Yu, M. F.; Files, B. S.; Arepalli, S.; Ruoff, R. S. *Phys. Rev. Lett.* **2000**, *84*, 5552.
4. Dyke, C. A.; Tour, J. M. *Chem. Eur. J.* **2004**, *10*, 813.
5. Song, Y. S.; Youn, J. R. *Carbon* **2005**, *43*, 1378.
6. Gojny, F. H.; Wichmann, M. H. G.; Fiedler, B.; Schulte, K. *Compos. Sci. Technol.* **2005**, *65*, 2300.
7. Gupta, M. L.; Sydlik, S. A.; Schnorr, J. M.; Woo, D. J.; Osswald, S.; Swager, T. M.; Raghavan, D. *J. Polym. Sci. B Polym. Phys.* **2013**, *51*, 410.
8. Lordi, V.; Yao, N. J. *J. Mater. Res.* **2000**, *15*, 2770.
9. Ma, P. C.; Siddiqui, N. A.; Kim, J. K. *Compos. A* **2010**, *41*, 1345.
10. Banerjee, S.; Benny, T. H.; Wong, S. S. *Adv. Mater.* **2005**, *17*, 17.
11. Salice, P.; Rossi, E.; Pace, A.; Maity, P.; Carofiglio, T.; Menna, E.; Maggini, M. *J. Flow Chem.* **2014**, *4*, 79.
12. Sydlik, S. A.; Lee, J. H.; Walish, J. J.; Thomas, E. L.; Swager, T. M. *Carbon* **2013**, *59*, 109.
13. Gojny, F. H.; Nastalczyk, J.; Roslaniec, Z; Schulte, K. *Chem. Phys. Lett.* **2003**, *370*, 820.
14. Thostenson, E. T.; Chou, T. W. *Carbon* **2006**, *44*, 3022.
15. Lau, K. T.; Lu, M.; Lam, C.; Cheung, H.; Sheng, F. L.; Li, H. L. *Compos. Sci. Technol.* **2005**, *65*, 2005.
16. Paiva, M. C.; Simon, F.; Novais, R. M.; Ferreira, T.; Proença, M. F.; Xu, W.; Besenbacher, F. *ACS Nano.* **2010**, *4*, 7379.
17. Boggs, M.; Li, M.; Beebe, T. P.; Huang, C. P. *Carbon* **2008**, *46*, 466.
18. Louette, P.; Bodino, F.; Pireaux, J.-J. *Surf. Sci. Spectra* **2005**, *12*, 8489.
19. Shen, J.; Huang, W.; Wu, L.; Hu, Y.; Ye, M. *Mat. Sci. Eng. A* **2007**, *464*, 151.
20. Grassi, G.; Scala, A.; Piperno, A.; Iannazzo, D.; Lanza, M.; Milone, C.; Pistone, A.; Galvagno, S. *Chem. Commun.* **2012**, *48*, 6836.
21. Voggu, R.; Das, B.; Rout, C. S.; Rao, C. N. R. *J. Phys. Condens. Matter* **2008**, *20*, 472204.
22. Bonifazi, D.; Nacci, C.; Marega, R.; Campidelli, S.; Ceballos, G.; Modesti, S.; Meneghetti, M.; Prato, M. *Nano Lett.* **2006**, *7*, 1408.
23. Dong, A.; Yu, Y.; Yuan, J.; Fan, X. *Appl. Surf. Sci.* **2014**, *301*, 418.
24. Georgakilas, V.; Bourlinos, A.; Gournis, D.; Tsoufis, T.; Trapalis, C.; Alonso, A. M.; Prato, M. *J. Am. Chem. Soc.* **2008**, *130*, 8733.
25. Chakraborty, A. K.; Plyhm, T.; Barbezat, M.; Necola, A.; Terrasi, G. P. *J. Nanopart. Res.* **2011**, *13*, 6493.
26. Hudson, J. L.; Casavant, M. J.; Tour, J. M. *J. Am. Chem. Soc.* **2004**, *126*, 11158.
27. Zeng, L.; Barron, A. R. *Nano Lett.* **2005**, *5*, 2005.
28. Baudot, C.; Volpe, M. V.; Kong, J. C.; Tan, C. M. US20090299082 A1.
29. Outouch, R.; Rauchdi, M.; Boualy, B.; El Firdoussi, L.; Roucoux, A.; Ali, M. A. *Acta Chim. Slov.* **2014**, *61*, 67.
30. Zhou, T.; Wang, X.; Liu, X. H.; Lai, J. Z. *eXPRESS Polym. Lett.* **2010**, *4*, 217.

31. Jin, F. L.; Ma, C. J.; Park, S. J. *Mat. Sci. Eng. A* **2011**, *528*, 8517.
32. Jee, A. Y.; Lee, M. *Curr. Appl. Phys.* **2011**, *11*, 1183.
33. Vennerberg, D.; Rueger, Z.; Kessler, M. R. *Polymer* **2014**, *55*, 1854.
34. Shen, J.; Huang, W.; Wu, L.; Hu, Y.; Ye, M. *Compos. Sci. Technol.* **2007**, *67*, 3041.
35. Shen, J.; Huang, W.; Wu, L.; Hu, Y.; Ye, M. *Compos. Part A* **2007**, *38*, 1331.